Int. J. Electrochem. Sci., 13 **(2018)** 1027 – 1041, doi: 10.20964/2018.01.50

International Journal of
ELECTROCHEMICAL
SCIENCE
www.electrochemsci.org

Effect of Calcination Time on Lithium Ion Diffusion Coefficient of $LiMg_{0.04}Mn_{1.96}O_4$ Prepared by a Solid-State Combustion Method

Tao Feng[1,2,3], *Wangqiong Xu*[1,2,3], *Xiaofang Liu*[1,2,3], *Miaomiao Shao* [1,2,3], *Junming Guo*[1,2,3,*], *Changwei Su*[1,2,3,*]

[1] Key Laboratory of Comprehensive Utilization of Mineral Resources in Ethnic Regions, Yunnan Minzu University, Kunming 650500, PR China
[2] Key Laboratory of Resource Clean Conversion in Ethnic Regions, Education Department of Yunnan, Yunnan Minzu University, Kunming 650500, PR China
[3] Joint Research Centre for International Cross-border Ethnic Regions Biomass Clean Utilization in Yunnan, Yunnan Minzu University, Kunming 650500, PR China
[*]E-mail: guojunming@tsinghua.org.cn ; abrastein@163.com

Received: 26 September 2017 / *Accepted:* 30 October 2017 / *Published:* 16 December 2017

A series of $LiMg_{0.04}Mn_{1.96}O_4$ cathode materials were prepared by a solid-state combustion method at temperature of 500°C for 1h and then calcined at 700°C for 3, 6, 9 and 12h. The effects of two-stage calcination time on structure, morphology, electrochemical properties and diffusion coefficient of lithium ions of $LiMg_{0.04}Mn_{1.96}O_4$ were studied. X-ray diffraction (XRD) results showed that the two-stage calcination time at 700°C is ineffective to change crystalline structure and phase composition, still retaining intrinsic spinel structure without any other impurity phases, but the crystallinity become well and particle size increases with calcination time increases. Scanning electron microscope (SEM) shows that $LiMg_{0.04}Mn_{1.96}O_4$ calcined at 700°C for 6h (LMMO-6h) has uniform, nearly octahedron structure morphology with narrow size distribution. Diffusion coefficient of lithium ions (D_{Li}^+) of $LiMg_{0.04}Mn_{1.96}O_4$ two-stage calcined at 700°C for 3-12 hours was calculated according to the charging peaks in cyclic voltammetric (CV) curves, it was found that the D_{Li}^+ value first increases and then slightly decreased with the calcined time at 700°C. The highest value of 7.19×10^{-11} and 7.48×10^{-11} cm^2 s^{-1} for the first and second oxidation peaks of LMMO-6h, respectively. The electrochemical tests also show LMMO-6h exhibited a better electrochemical than other samples.

Keywords: $LiMg_{0.04}Mn_{1.96}O_4$; solid-state combustion method; diffusion coefficient; calcination time; lithium ion batteries

1. INTRODUCTION

Spinel lithium manganese oxide because of their high working voltage, low cost, low-toxicity and environmental friendliness have been studied extensively as one of the most promising cathode

materials for lithium-ion batteries[1-6]. However, $LiMn_2O_4$ suffers from severe capacity loss such as Jahn-Teller distortion[7], the dissolution of manganese in the electrolyte[8], electrolyte decomposition at the electrode in the process of charge and discharge[9] and so on.

To overcome the Jahn-Teller distortion, researchers usually using cationic doping to substitute Mn ions on 16d octahedral sites, so that improve the stability of lithium manganate positive electrode material. Such as Li^+, Zn^{2+},Si^{4+}, Al^{3+}, Cr^{3+}, Mg^{2+} and Ni^{2+} [10-15] could increase the average state of Mn ions, enhance structural stability of MnO_6 octahedron and suppress the lattice distortion[16-19]. Especially $LiMg_xMn_{2-x}O_4$ enables the more prominent discharge capacity and cycling stability due to the higher strength of Mg-O bonding compared to that of the Mn-O bond[20]. Huang et al. [21] synthesized a $LiMg_{0.05}Mn_{1.95}O_4$ cathode material at a low temperature of 400°C for 1h and 600°C for 3h by a molten-salt combustion processing, which get an improved initial discharge capacity of 122 mAh g^{-1} at 0.5C. Zhao et al. [22] synthesized Mg-doped $LiMg_{0.06}Mn_{1.94}O_4$ cathode material using a citric acid-assisted sol-gel synthesis method. They show that sample exhibited the higher initial capacity of 120.5 mAh g^{-1} and capacity retention reached 98％ after 30 cycles at 0.5C showing excellent cycling performance and illustrate that doped with Mg could significantly improve the crystals structural stability.

The synthesis method also can influence the quality of $LiMn_2O_4$ powders used for lithium-ion batteries[23]. However, conventional and commercial spinel $LiMn_2O_4$ is synthesized by a high temperature solid-state reaction, which has some disadvantage such as requires high temperature and long heating time[24]. Cai et al.[25] prepared the $LiMn_2O_4$ by solid-state combustion at temperature of 350°C for 2h and then calcined at 800°C for 10h. The initial discharge capacity of the synthesized materials was found to be 107.9 mAh g^{-1} and present a remarkable cycling performance with capacity retention of 76.27% after 1000 cycles at 5C. Xiang et al.[26] have reported that the $LiMg_{0.08}Mn_{1.92}O_4$ is synthesized by solid-state combustion at a low temperature of 500°C for 1h. It shows a better cycling stability. Based on these examples, we found that solid-state combustion synthesis has some remarkable advantages such as saves reaction time and lower reaction temperature[23].

In this paper, the $LiMg_{0.04}Mn_{1.96}O_4$ cathode materials were prepared by a solid-state combustion method preheated to 500°C for 1h and then calcined at 700°C for 3h, 6h, 9h and 12h with manganese carbonate and lithium carbonate as raw materials, magnesium acetate as Mg^{2+} dopant and citric acid as a fuel. The relation between the calcination time and morphology, electrochemical behavior was investigated. We have analyzed the diffusion coefficient of lithium of samples for different two-stage calcination times and different charge depth and got a preliminary understanding of the influence between calcination time, D_{Li}^+ value and the electrochemical performance.

2. EXPERIMENTAL

2.1. Synthesis of $LiMg_{0.04}Mn_{1.96}O_4$

$LiMg_{0.04}Mn_{1.96}O_4$ was prepared by the solid-state combustion synthesis. lithium carbonate (AR, Sinopharm Chemical reagent Co., Ltd.), manganese carbonate (AR, alading) and magnesium acetate (AR, Sinopharm Chemical reagent Co.,Ltd.) which were weighed according to a stoichiometric molar ratio Li:Mn:Mg=1:1.96:0.04 with a total mixture mass of 30g, and placed in a 500ml

polytetrafluoroethylene jar. A fuel of 1.5g citric acid (AR, Sinopharm Chemical reagent Co., Ltd.) was then added to the jar. The mixture was ball-milled thoroughly by planetary ball mill with ethanol as a medium. The obtained precursor (off-white) powders were then heated in a convection oven at 80°C. Subsequently, about 5.5g of the precursor mixture was placed in an alumina crucible and calcined in a muffle furnace at 500°C for 1h in air. And then cool the one-stage calcined $LiMg_{0.04}Mn_{1.96}O_4$ materials to ambient temperature. After grinding the samples, then the materials were calcined in the muffle furnace at 700°C for 3h, 6h, 9h and 12h in air, respectively. The two-stage calcined materials in black powders were obtained after cooling naturally to ambient temperature.

2.2 Characterization

The crystal properties of $LiMg_{0.04}Mn_{1.96}O_4$ were examined with an X-ray Diffractometer (XRD, D/max-TTRIII, Japan) with Cu Kα radiation at a voltage of 40Kv and a current of 30mA. XRD spectra were obtained at 2θ angles of 10° to 70° with a scanning step of 0.02° and a scanning speed of 4° min^{-1}. Lattice parameters were obtained by means of the Jade 5.0 software. The morphology of the $LiMg_{0.04}Mn_{1.96}O_4$ particles and the surface morphologies of the pristine were observed using a scanning electron microscopy (SEM, QUANTA-200 American FEI Company).

2.3 Electrochemical studies of active materials

For electrochemical studies, composite electrodes were fabricated with the active material, polyvinylidene fluoride (PVDF) and the acetylene black in the mass rate 80:10:10 using N-methy-2-pyrrolidinone (NMP) as solvent for the binder. Spreading uniformly on an aluminum foil using doctor-blade technique drying in an convection oven at 80°C for 4h. The dried electrode film was punched into discs (16mm diameter) forming the test cathode. Lithium metal foil, 1M $LiPF_6$ in ethylene carbonate (EC)-1,2-dimethyl carbonate (DMC) as the electrolyte (EC and DMC volume ratio of 1:1) and Celgard 2320-type membrane as the separator ,respectively to assemble coin-type cells (CR2025) in a dry glove box filled with high purity argon gas. The weight of active material per cm^2 was about 2mg. Charge/discharge cycling at constant current mode was carried out using a Land electric test system CT2001A (Wuhan Jinnuo Electronics Co., Ltd.) at room temperature and cyclic voltammogram texts were carried out on ZAHNER Zennium IM6 Electrochemical Workstation (ZAHNER-elektrik GmbH & Co. KG, Kronach, Germany) from 3.60 to 4.50V (vs. Li/Li^+) with a scan rate of 0.02mV s^{-1}.

3. RESULTS AND DISCUSSION

3.1. Structure and morphology

Fig. 1 and Table 1 shows the XRD patterns and lattice parameters of the $LiMg_{0.04}Mn_{1.96}O_4$ annealing at 500°C for 1h and two-stage calcination at 700°C for 3, 6, 9, 12h. It is found the characteristic diffraction peaks of the cubic spinel $LiMn_2O_4$ with the Fd3m space group (PDF35-0782),

corresponding to eight typical crystal planes of (111), (311), (222), (400), (331), (511), (440) and (531). No impurity is detected, indicating that the addition of Mg ions did not change the spinel structure of $LiMn_2O_4$. Meanwhile, substitution of manganese with magnesium should result in a shrinkage of the lattice parameters. This is mainly because the Mg^{2+} occupation in the crystal, reduce the content Mn^{3+} ions in bulk $LiMn_2O_4$ and the ionic radius of the Mn^{3+} ions (0.66Å) is higher than that of Mn^{4+} (0.60Å)[27]. The lattice parameters of samples first decreases and then increases with the two-stage calcination time increases. What's more, the lattice parameters of all samples were less than the standard value 8.247Å of spinel $LiMn_2O_4$, which indicated that Mg ions were incorporated into the spinel $LiMn_2O_4$ lattice. The LMMO-6h exhibits the highest intensity ratio of (311)/(400) peaks, as shown in Table 1. This indicates that sample can present good electrochemical performance[28]. But with two-stage calcination time increases, the full width at half maximum (FWHM) of (400) peaks became narrower, and the minimum values are reached at 12h. Indicating better crystallinity for $LiMg_{0.04}Mn_{1.96}O_4$ with the time increased gradually.

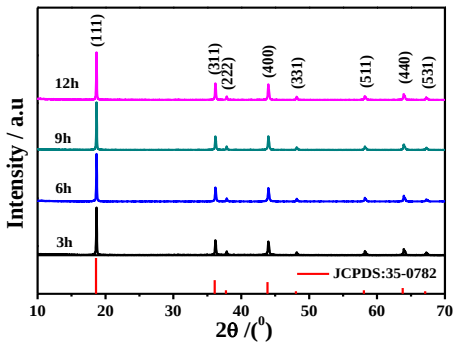

Figure 1. XRD pattern of the $LiMg_{0.04}Mn_{1.96}O_4$ at 700°C for 3h, 6h, 9h and 12h in air.

Table 1. The lattice parameters of $LiMg_{0.04}Mn_{1.96}O_4$.

two-stage calcination time (h)	Lattice constant (Å)	FWHM (400) peak (°)	Intensity ratio of (311)/(400) peaks
3	8.2382	0.228	0.96
6	8.2373	0.215	1.02
9	8.2374	0.209	0.92
12	8.2378	0.204	0.95

The SEM images of the $LiMg_{0.04}Mn_{1.96}O_4$ powders are shown in Fig. 2. It can be seen that all the samples are composed of agglomerated structure. However, the agglomerate decreases with the increase of calcination time. The sample become larger with two-stage calcination time increases and the sizes changed to greater due to particle growth and showed the regular octahedron structure clearly, implying that the increase of two-stage calcination time can effectively promote the growth of grains. The diameter of the micron-sized secondary particles is about 0.1~0.5μm. It has been suggest that

better crystallinity and moderate particle size may improve the electrochemical performance of $LiMn_2O_4$ [29].

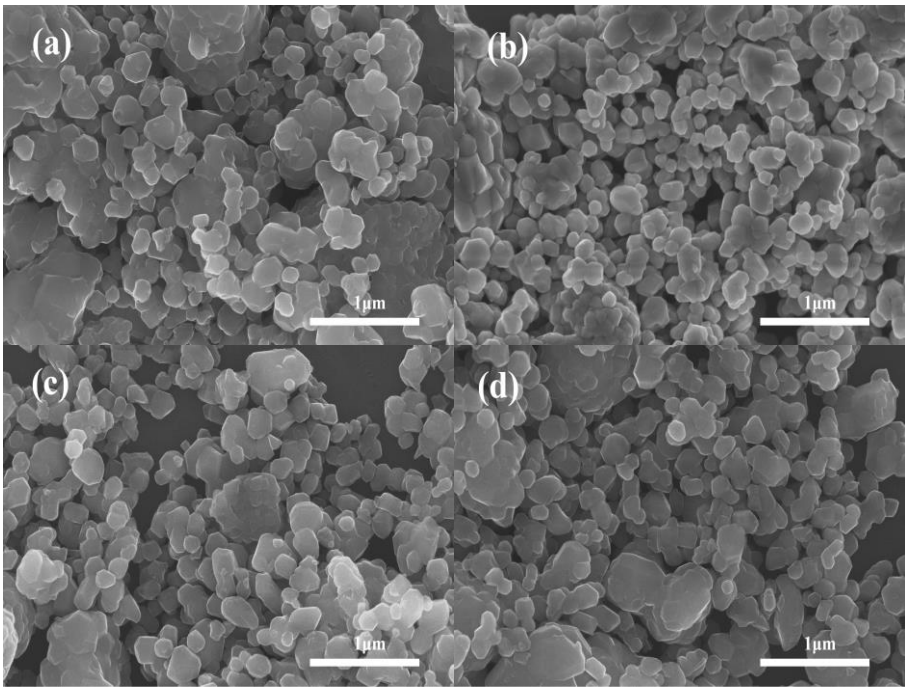

Figure 2. SEM images of the $LiMg_{0.04}Mn_{1.96}O_4$ at 700°C for different heat treatment time in air (a)3h, (b)6h, (c)9h, (d)12h.

3.2. Electrochemical characterization

The initial charge-discharge curves of different two-stage calcination time samples are shown in Fig. 3(a) at current density of 1C between the potential range 3.0-4.5V (vs Li/Li^+) at room temperature. On the charging process, there is a sudden increase in voltage to 4.0 V from the open-circuit voltage, followed by two well defined plateau regions are observed for all compounds corresponding to the Li de-insertion/insertion process.

The cycling performance of $LiMg_{0.04}Mn_{1.96}O_4$ samples at the different calcination time at 1C rate and in the voltage range of 3.00-4.50V at the room-temperature in Fig. 3(b). The initial and 1000^{th} discharge specific capacities and capacity retention rates of the samples are summarized in table 2. From Fig. 3(b) and table 2, we note that the initial discharge specific capacity and capacity retention tend to increase first and then reduce after the increase with the increase of two-stage calcination time. The sample LMMO-6h has the highest initial discharge specific capacities are 123.9 mAh g^{-1}, then the samples' highest initial discharge specific capacities decrease with the second roasting time increase. This is because increasing the calcination time is in favor of the secondary nucleation and morphology control of the primary particles to obtain the micro-sized structure, which provide a relatively short distance and low resistance for Lithium-ion migration, facilitating the fast charge–discharge characteristics[30]. However, the increase of calcination time can also promote the sample have larger particle size, causing long lithium diffusion path.

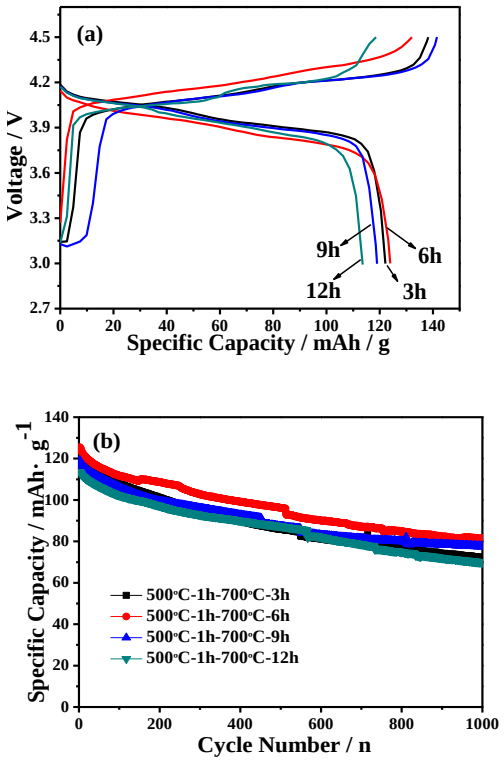

Figure 3. The initial charge-discharge curves (a) and Cyclic performances (b) of $LiMg_{0.04}Mn_{1.96}O_4$ samples at different two-stage calcination time.

Table 2. Discharge specific capacity and capacity retention rate of $LiMg_{0.04}Mn_{1.96}O_4$ samples at 1C rate under room temperature.

two-stage calcination time (h)	Discharge capacity (mAh g^{-1})		Capacity retention rate(%)
	Initial	1000^{th}	
3	122.1	72.3	59.21
6	123.9	81.4	65.70
9	119	77.9	65.46
12	113.6	69.7	61.36

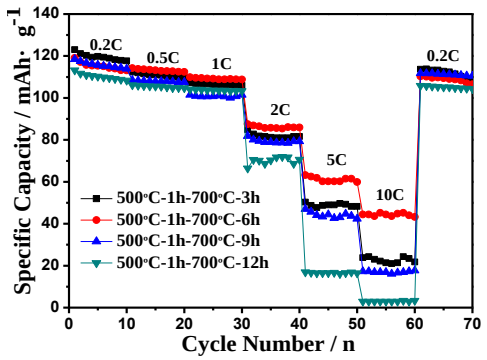

Figure 4. Specific capacity vs. cycle number of $LiMg_{0.04}Mn_{1.96}O_4$ prepared at different two-stage calcination time and at various current rate ranging from 0.2C to 10C.

The path of lithium diffusion is too long may hinder the diffusion of lithium ion. The sample of 6h delivers the highest initial specific capacity and discharge specific capacities of 81.4mAh g^{-1} with the capacity retention of 65.70% after 1000^{th} cycles. Therefore the $LiMg_{0.04}Mn_{1.96}O_4$ sample at two-stage calcination time 6h has best the initial specific capacity and capacity retention.

Fig. 4 displays the rate capabilities of the $LiMg_{0.04}Mn_{1.96}O_4$ prepared at different two-stage calcination time at varying rates from 0.2C to 10C and back to 0.2C in the voltage range of 3.0~4.5V at room temperature. It can be observed that the discharge capacity all decreases with the rate increase due to electrochemistry polarization. The LMMO-6h is found to have higher discharge capacity and capacity-retention values at 0.5C to 10C rates. For example, at 10C rates, capacities of 44.5(±1) mAh g^{-1} are measured, which are stable at least up to 10 cycles. When decreasing current rate from 10C to 0.2C, the discharge capacities of the four cathode materials are almost restored to their initial discharge capacities at 0.2C, which indicating their good electrochemical reversibility. Compared with the four cathode materials, it can be seen that the LMMO-6 has better rate performance than other samples.

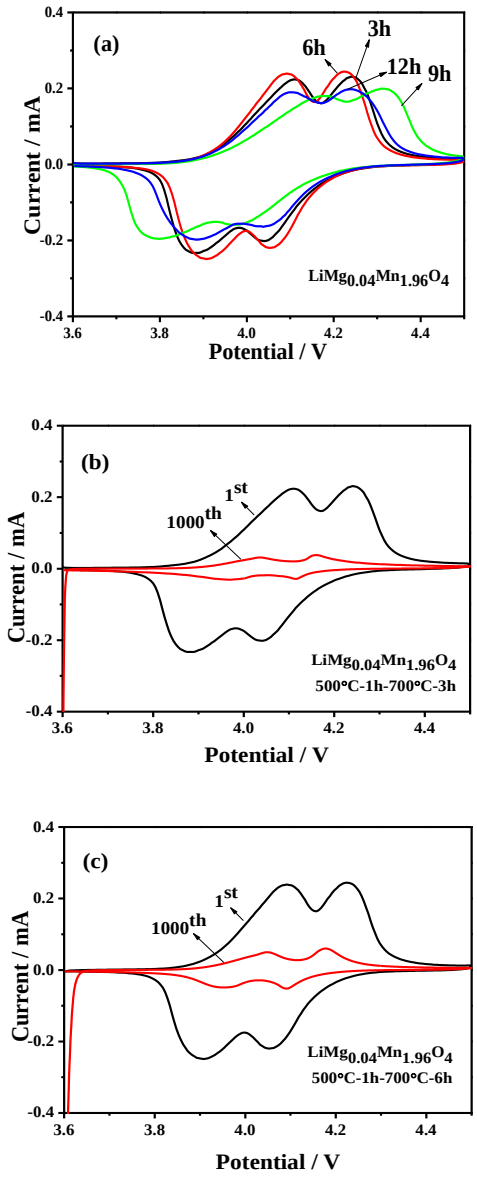

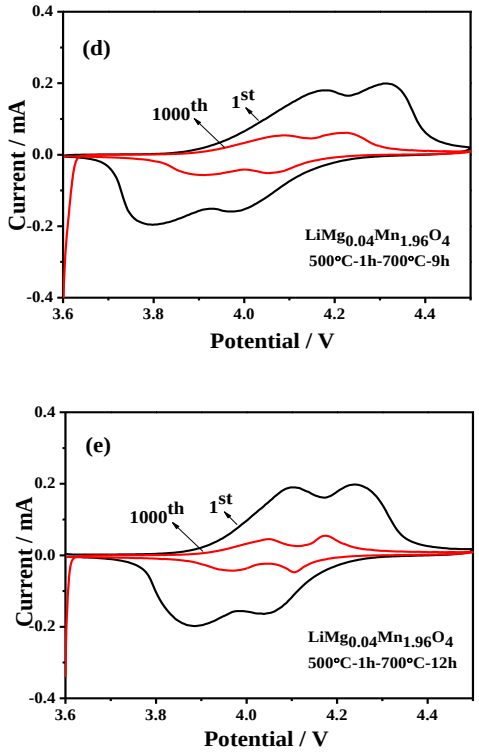

Figure 5. Cyclic voltammetric (CV) curves (a) of the $LiMg_{0.04}Mn_{1.96}O_4$ of different two-stage calcination time at 1st cycle and after 1000th cycles: (b) 3h, (c) 6h, (d) 9h and (e) 12h in the potential rang of 3.6-4.5V (vs. Li/Li^+) at a scan rate of 0.02 mV s^{-1}.

To investigate the reversibility of the electrodes, cyclic voltammetry (CV) was measured for the four electrodes after 1st, and 1000th in the potential rang of 3.6-4.5V (vs. Li/Li^+) at a scan rate of 0.02mVs^{-1} at room temperature. Fig. 5(a) shows cyclic voltammogram curves of the $LiMg_{0.04}Mn_{1.96}O_4$ sample at 1st cycle. Two pairs of redox peaks appear in the CVs, which locate at 4.10V/3.90V and 4.20V/4.00V for all samples. The two pairs of redox peaks are consistent with the two potential plateaus of the charge-discharge curves in Fig. 3(a). It is known that, these two pairs of current peaks originate from two reversible phase–phase transitions of the $LiMn_2O_4$ during lithiation and delithiation processes[31]. The separation of anodic and cathodes peaks for $LiMg_{0.04}Mn_{1.96}O_4$ are 0.20V and 0.22V for 3h, 0.17V and 0.18V for 6h, 0.33V and 0.37V for 9h, 0.20V and 0.21V for 12h. It can be seen that the sample of 6h shows smaller potential difference, indicating faster lithium intercalation/de-intercalation and higher reversibility of electrode reaction in the latter. Fig. 5(b), (c), (d) and (e) comparatively illustrate the CV curves of the $LiMg_{0.04}Mn_{1.96}O_4$ electrodes at 1st cycle and after 1000th cycles, respectively. For the all samples, the two pairs of redox peaks are linked most strongly with the reversible lithiation and delithiation processes of lithium ions. After 1000th cycles, the corresponding peak currents are reduced evidently, but still exhibits two pairs of obvious redox peaks. The results indicate that the Mg-doping can effectively improve the reversibility and reduce the polarization of electrode. Apart from that, the CV curves of LMMO-6h displays higher current densities and smaller potential difference after 1000th cycles. This demonstrated that the LMMO-6h have an superior reversibility and smaller polarization of electrode than other samples, even after 1000th cycles.

As far as we all know, the diffusion of Li^+ ion is the rate-determining step during reaction on the charging and discharging process[32]. Therefore, it is an important factor to influence the LMn_2O_4 cathode materials. The lithium diffusion coefficient can be calculated from Eq.(1) at room temperature[33].

$$I_p = 2.69\times10^5\times n^{3/2}\times A\times D_{Li}^{1/2}\times C_o\times v^{1/2} \quad (1)$$

Where I_p is the peak current, n is the electron transfer number of the reaction, A is the surface area of the electrode, D_{Li}^+ is the diffusion coefficient of Li^+, v is the scan rate, and C_o is the bulk concentration of Li^+ in the electrode, respectively. Fig. 6(a-d) shows the cyclic voltammograms of the $LiMg_{0.04}Mn_{1.96}O_4$ sample at different calcination time at different sweep rates of 0.02, 0.05, 0.10, 0.15, 0.20mV s^{-1} ranging from 3.6V to 4.5V, respectively. It can be seen that the potential of anodic and cathodic peaks become larger with the increased scan rate for all samples. Even at a high scan rate of 0.2mV s^{-1}, $LiMg_{0.04}Mn_{1.96}O_4$ sample still presents two couples of well separated redox peaks. It indicates that the samples possess better electrochemical reversibility.

The D_{Li} can be calculated from the slop of I_p vs. $v^{-1/2}$ plots as shown in Fig. 6(e-h). The all of D_{Li}^+ value of samples are given in Table 3. As can be seen from the Table 3, the lithium diffusion values fall within the order of 10^{-11} cm^2 s^{-1}. We found the D_{Li} value first increases and then slightly decreases with the two-stage calcination time increases, correspond to the variation of lattice parameter. It is because the LMMO-6h has more uniform distribution and better-grown crystal, which providing more storage sites of Li^+ ions and spacious channel for lithium ion diffusion[32]. However, after the calcination time exceeds 6 hours, the D_{Li}^+ value of samples descend. It is due to the larger crystals provide a longer diffusion length and it is disadvantage for ions migration. The LMMO-6h has the highest D_{Li}^+ value with two oxidation peak of A_1(7.19×10^{-11} cm^2 s^{-1}) and A_2 (7.48×10^{-11} cm^2 s^{-1}), which are similar with the pure $LiMn_2O_4$ synthesized by high temperature solid-state combustion reaction using cellulose as fuel[34]. Thus it can be concluded that the LMMO-6h has reasonable particle size and shorter diffusion length, show a better performance than other samples. However, the calculation results of D_{Li}^+ value of all samples are slightly lower than $LiAl_{0.03}Mn_{1.97}O_4$ prepared by the PVP-assisted gel combustion method[35].

Interestingly, compare the all samples, we found that the diffusion coefficient of Li^+ ion from the oxidation peak at high potential is larger than that at lower potential. In other words, D_{Li}^+ increases slightly with the increase of charge depth. This phenomenon may be due to reconstruction of the interface layer on the electrode surface caused by contraction and expansion of the cell volume during the processes of lithiation and delithiation[36]. In the charging processes, the de-intercalation of Li^+ ion is decrease the electrode volume and the surface layer. These changes reducing the resistance for lithium ion migration[37].

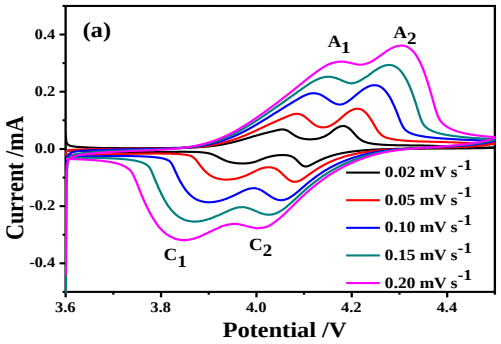
(a)
A1
A2
C1
C2
0.02 mV s-1
0.05 mV s-1
0.10 mV s-1
0.15 mV s-1
0.20 mV s-1
Current /mA
Potential /V

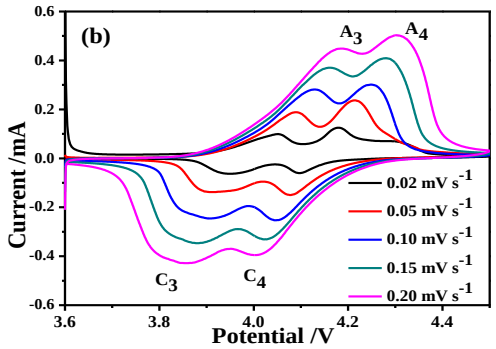
(b)
A3
A4
C3
C4
0.02 mV s-1
0.05 mV s-1
0.10 mV s-1
0.15 mV s-1
0.20 mV s-1
Current /mA
Potential /V

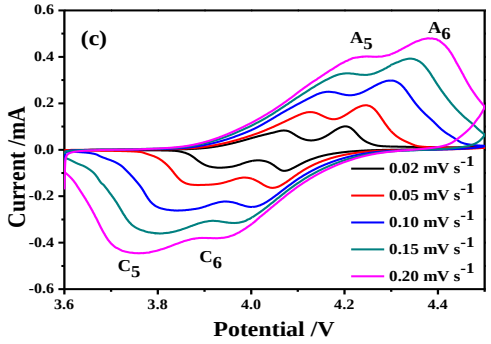
(c)
A5
A6
C5
C6
0.02 mV s-1
0.05 mV s-1
0.10 mV s-1
0.15 mV s-1
0.20 mV s-1
Current /mA
Potential /V

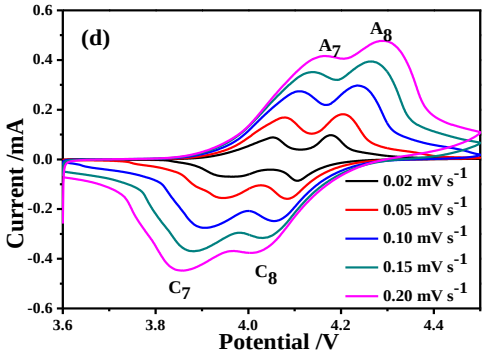
(d)
A7
A8
C7
C8
0.02 mV s-1
0.05 mV s-1
0.10 mV s-1
0.15 mV s-1
0.20 mV s-1
Current /mA
Potential /V

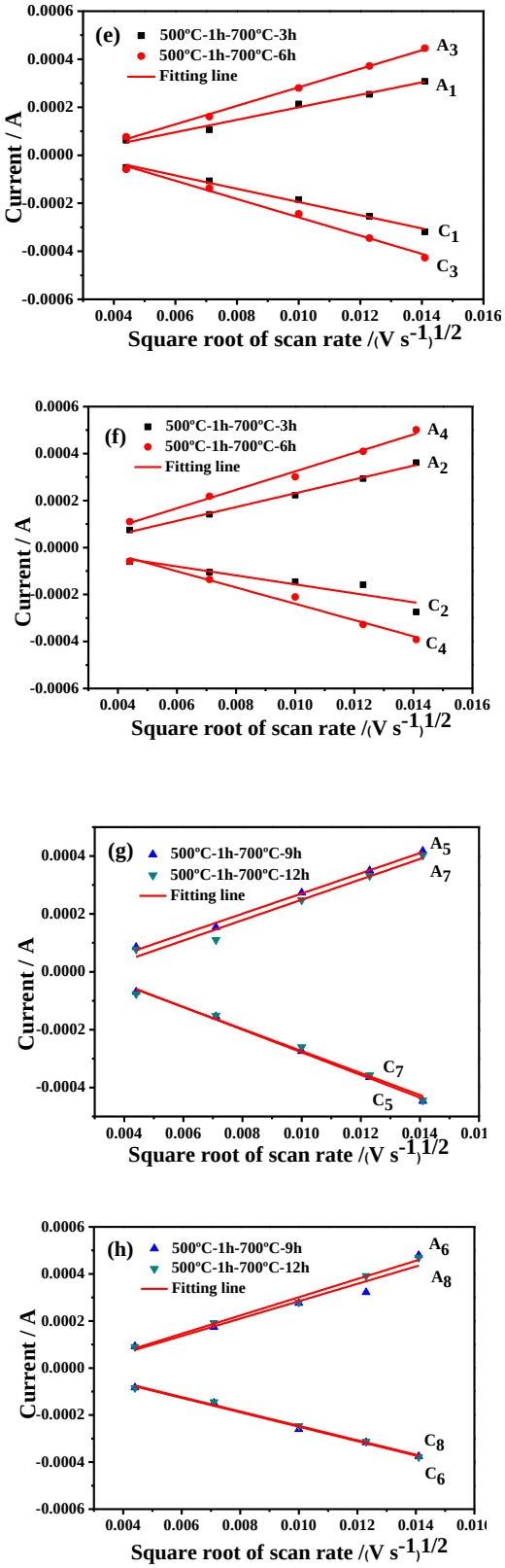

Figure 6. (a)-(d) different two-stage calcination time samples electrodes in the potential rang of 3.6-4.5V (vs. Li/Li^+) at various scan rates ranged from 0.02 to 0.2 mV s^{-1}, (e)-(h) plots of peak current vs. Square root of the scan rate for different calcination time samples.

Table 3. Li^+ diffusion coefficient of different two-stage calcination time $LiMg_{0.04}Mn_{1.96}O_4$

two-stage calcination time (h)	Peak	Li^+ diffusion coefficient, D_{Li^+} ($cm^2\ s^{-1}$)
3	A_1	3.26×10^{-11}
	A_2	4.19×10^{-11}
6	A_3	7.19×10^{-11}
	A_4	7.48×10^{-11}
9	A_5	6.03×10^{-11}
	A_6	7.01×10^{-11}
12	A_7	5.92×10^{-11}
	A_8	6.29×10^{-11}

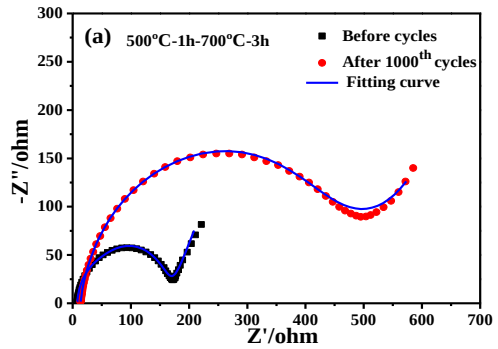

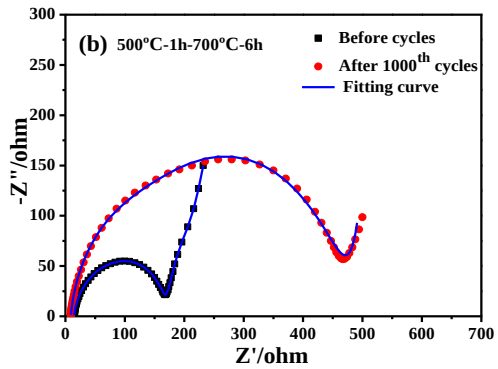

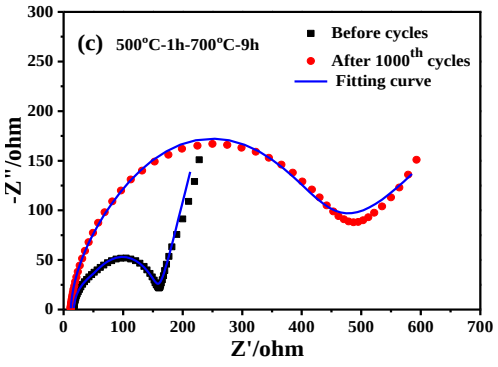

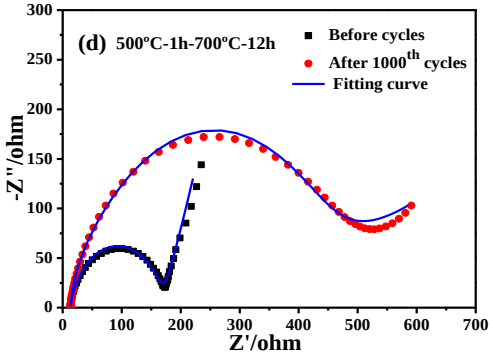

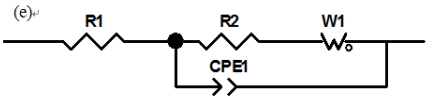

Figure 7. (a)-(d) Electrochemical impedance spectra of the $LiMg_{0.04}Mn_{1.96}O_4$ samples at different two-stage calcination time before cycles and after 1000^{th} cycles at room temperature, (e) Equivalent circuit model of EIS.

Table 4. Fitting values of the charge transfer resistance (R_{ct}) obtained from EIS.

two-stage calcination time (h)	R_{ct} (Ω)	
	before cycles	after 1000^{th} cycles
3	166	464
6	171	451
9	159	462
12	170	475

Nyquist plots (Fig. 8) and fitting results (Table 4) of the $LiMg_{0.04}Mn_{1.96}O_4$ samples at different two-stage calcination time are displayed. The plots are modeled by the equivalent circuit Fig.7(e) by Zview software. Fig. 7 (a-d) shows the impedance of different calcination time samples before and after 1000^{th} cycles. Obviously, all of the samples contain two partial, a semicircle in the high frequencies and a straight slopping line in low frequencies. R_1 is the resistance of lithium-ion migration through the SEI film. The symbols, R_{ct}, W_1, C_1, Represent the charge transfer impedance, Warburg impedance, reflection of intercalation capacitance, respectively[38]. From the results, we can see that the LMMO-6h has the highest resistance (171Ω) before cycles. However, after 1000 cycles, this sample presents the lowest R_{ct} (451Ω), implying the small R_{ct} is favorable to a faster reaction rate of lithium ions in the charge/discharge process and better electrochemical performance[39].

4. CONCLUSIONS

The spinel $LiMg_{0.04}Mn_{1.96}O_4$ cathode materials were prepared by a solid-state combustion method at temperature of 500°C for 1h and then calcined at 700°C for different times. XRD indicates that the particle size of the $LiMg_{0.04}Mn_{1.96}O_4$ become larger with increasing the two-stage calcination time and the crystallinity become well due to particle growth and showed the grains are of micron size. The $LiMg_{0.04}Mn_{1.96}O_4$ spinel powder with various particle sizes can be obtained by controlling the calcination time. Compared with all samples, LMMO-6h exhibited the optimal capacity retention with the highest initial discharge specific capacity of 123.9mAh g^{-1} after 1000 cycles at 1C at 24°C. The calculate results also suggested that the LMMO-6h shows the highest D_{Li}^+ value with two oxidation peak of A_1(7.19×10^{-11} cm^2 s^{-1}) and A_2 (7.48×10^{-11} cm^2 s^{-1}), respectively. These results indicated that the effect of the reasonable calcination time for the preparation of $LiMn_2O_4$ cathode materials with high performance.

ACKNOWLEDGEMENTS
This work was financially supported by the National Natural Science Foundation of China (51462036, U1602273), Innovation Program of Yunnan Minzu University (2016YJCXS18).

References

1. C.R. Xu, Y.J. LU, H. Hu, P.L. Li, L. Kong, Q.Y. Su and X.L. Cao, *Int. J. Electrochem. Sci*., 12 (2017) 5185-5198.
2. Y.L. Ding, J. Xie, G.S. Cao, T.J. Zhu, H.M. Yu and X.B. Zhao, *J. Phys. Chem*. C., 115 (2011) 9821-9825.
3. O.K. Park, Y. Cho, S. Le, H.C. Yoo, H.K. Song and J. Cho, *Energ Environ Sci.*, 4 (2011)16-21.
4. K. Kang, Y.S. Meng, J. Breger, C.P. Grey and G. Ceder, *Science*, 311 (2006)977-980.
5. Z.J. Zhang, S.L. Chou, Q.F. Gu, H.K. Liu, H.J. Li, Kiyoshi Ozawa and J.Z. Wang, *ACS Appl. Mater. Interfaces*, 6 (2014) 22155.
6. W.Q. Xu, J.J. Huang, Q.L. Li, H.L. Bai, C.W. Su, Y.H. He, W. Bai and J.M. Guo, *Int. J. Electrochem. Sci*., 10 (2015) 9351-9358.
7. R.J. Gummow, A.D. Kock and M.M. Thackeray, *Solid State Ionics*, 69 (1994) 59-67.
8. X. Li and Y. Xu, *Electrochemistry Communications*, 9 (2007) 20-23.
9. Y.Y. Xia, Y.H. Zhou and M. Yoshio, *J. Electrochem. Soc*., 144 (1997) 25-93.
10. R. Thirunakaran, T. Kim and W.S. Yoon, *Particuology*, 24 (2016) 87-95.
11. R.J. Gummow and Y. He, *J. Power Sources*, 253 (2014) 315-331.
12. H. Zhao， S. Liu， Z. Wang， Y. Cai and M. Tan, *Ceram. Int.*, 42 (2016) 13442-13448.
13. B. Shen, P. Zuo and Q. Li, *Electrochim. Acta*, 224 (2017) 96-104.
14. R. Thirunakaran, K.T. Kim, Y.M. Kang and J.Y. Lee, *Mater Res Bull*,40 (2005) 177-186.
15. X. Gu, X.W. Li, L.Q. Xu, H.Y, Xu, J. Yang and Y.T. Qian, *Int. J. Electrochem. Sci*., 7 (2012) 2504-2512.
16. R. Santhanam and B. Rambabu, *J. Power Sources*,195 (2010) 5442–5451.
17. C.Y. Ouyang, X.M. Zeng, Z. Sljivancanin and A. Baldereschi, *J. Phys. Chem*. C, 114 (2010) 47-56.
18. G.G. Amatucci, C.N. Schmutz, A. Blyr, C. Sigala, A.S. Gozdz, D. Larcher and J.M. Tarascon, *J. Power Sources*, 69 (1997) 11-25.
19. M.C. Smart, B.V. Ratnakumar, J.F. Whitacre, L.D. Whitcanack, K.B. Chin, M.D. Rodriguez, D. Zhao, S.G. Greenbaum and S. Surampudia, *J. Electrochem. Soc*.,152 (2005) A1096-A1104
20. H. Zhang, D. Liu, X.S. Zhang, C.J. Zhao and Y.L Xu, *J. Solid State Electr.*, 18 (2014) 569–575.
21. J.J. Hang, F.L. Yang, Y.J. Guo, C.C. Peng, H.L. Bai, J.H. Peng and J.M. Guo, *Ceram. Int.*, 41 (2015) 9662–9667.
22. H.Y. Zhao, X.Q. Liu, C. Cheng, Q. Li, Z. Zhang, Y. Wu, B. Chen and W.Q. Xiong, *J. Power Sources*, 282 (2015) 118-128.
23. P. Shen, D. Jia and Y. Huang, *J. Power Sources*, 158 (2006) 608-613.
24. H.S. Zhou, J. Xie, X.H. Xie, G.S. Tang and K.B. Li, *Integrated Ferroelectrics*, 147 (2013) 1–7.
25. Y. Cai, Y. Huang, X. Wang, *Ceram. Int.*, 40 (2014) 14039-14043
26. M.W. Xiang, L.Q. Ye, C.C. Peng, L. Zhong, H.L. Bai, C.W. Su and J.M. Guo, *Ceram. Int.*, 40 (2014) 10839-10845.
27. S. Mukerjee, X.Q. Yang and X. Sun , *Electrochim. Acta*, 49 (2004) 3373-3382.
28. Y.S. Lee, N. Kumada and M. Yoshio, *J. Power Sources*, 96 (2001) 376-384.
29. G.H. Jin, H. Qiao, H.L. Xie, H.Y. Wang, K.J. He and P. Liu, *Electrochim. Acta*, 150 (2014) 1-7.
30. Z. Zhang, Z. Chen and G. Wang , *Phys. Chem. Chem. Phys.*, 18 (2016) 68-93.
31. A. Sakunthala, M.V. Reddy, S. Selvasekarapandian, B.V.R. Chowdari and P.C. Selvin, *Electrochim. Acta*, 75 (2012) 118-119.
32. K.T. Lee and *J. Cho. Nano Today*, 6 (2011) 28–41.

33. J.L. Wang, Z.H. Li, J. Yang, J.J. Tang, J.J. Yu, W.B. Nie, G.T. Lei and Q.Z. Xiao, *Electrochim. Acta*, 75 (2012) 115-122.
34. Y.J. Cai, Y.D. Huang, X.C. Wang, D.Z. Jia, W.K. Pang, Z.P. Guo, Y.P. Du and X.C. Tang, *J. Power Sources*, 278 (2015) 574-581.
35. K.H. Dai, J. Mao, Z.T. Li, Y.C. Zhai, Z.H. Wang, X.Y. Song and V. Battaglia, G. Liu, *J. Power Sources*, 248 (2014) 22-27.
36. S.J. Bao, Y.Y. Liang and W.J. Zhou, *J. Power Sources*, 154 (2006) 239-245.
37. M. Prabu, M.V. Reddy and S. Selvasekarapandian, *Electrochim. Acta*, 88 (2013) 745-755.
38. R.H. Zeng, W.S. Li, D.S. Lu, Q.M. Huang and L.Z. Zhao, *T. Nonferr Metal Soc.*, 17 (2007) 1312-1318.
39. Z.D. Peng, Q.L. Jiang, K. Du, W.G. Wang, G.R. Hu and Y.X. Liu, *J. Alloys Compd.*, 493 (2010) 640–644.